A Combined Experimental and Simulation Study of Amplitude Modulation Atomic Force Microscopy Measurements of Self-Assembled Monolayers in Water

Xiaoli Hu[†], *Warren Nanney*[‡], *Kenichi Umeda*[§], *Tao Ye*[‡*], *Ashlie Martini*[†*]

[†]Department of Mechanical Engineering, University of California Merced, 5200 N Lake Road, Merced, CA 95343, United States

[‡]Chemistry and Chemical Biology, University of California Merced, 5200 N Lake Road, Merced, CA 95343, United States

[§]Department of Advanced Materials Science, The University of Tokyo, 7 Chome-3-1 Hongo, Bunkyō, Tokyo 113-8654, Japan

ABSTRACT

Atomic force microscopy (AFM) can be used to measure surface properties at the nanoscale. However, interpretation of measurements from amplitude modulation AFM (AM-AFM) in liquid is not straightforward due to the interactions between the AFM tip, the surface being imaged and the water. In this work, amplitude-distance measurements and molecular dynamics simulations of

AM-AFM were employed to study the effect of surface hydrophobicity on the amplitude of tip oscillation in water. The sample surfaces consisted of self-assembled monolayers where the hydrophilicity or hydrophobicity was determined by the terminal group of the alkanethiols. Analysis showed that surface chemical composition influences the hydration structure near the interface which affects the forces experienced by the tip and in turn changes the amplitude profile. This observation could aid our understanding of AM-AFM measurements of interfacial phenomena on various surfaces in water.

INTRODUCTION

Atomic force microscopy (AFM) has been widely used to measure the nanoscale topography and surface properties of materials in different environments, including in liquid.[1-11] The ability of AFM to probe surfaces in liquid is particularly important to studies of corrosion, lubrication, electrochemistry and biomaterials.[12] Amplitude modulation AFM (AM-AFM), a dynamic AFM mode that uses tip oscillation amplitude as the feedback, has been shown to reach atomic resolution in a liquid environment.[7, 13-16] However, a challenge is that the imaging mechanisms, *i.e.*, how the imaging contrast is ultimately determined by the atomic scale interactions between the tip apex and the surface, are not well understood, limiting improvements in the reproducibility of imaging and the interpretation of results.[13, 17-18] Compared to measurements in air or vacuum, the solid/liquid interfacial structure in a liquid environment can introduce additional complexity for AM-AFM. For example, water is known to form hydration layers due to interactions with adjacent surfaces.[19] These layers resulted in oscillatory forces in previous AFM measurements of surfaces in water.[8, 11, 14-16, 20-21] Oscillatory force profiles have also been found in molecular dynamics (MD) simulations of solid/liquid interfaces, and these simulations provided atomic-level information about the hydration structure.[22-25] Some studies suggested that atomic scale contrast originates from water

molecules bound to the surface functional groups.[26] However, to the best of our knowledge, there has been no direct correlation between hydration structure, interaction forces and the measured amplitude in AM-AFM. Further, it is not clear how functional groups on the surface influence the hydration structure and tip-surface interactions.[27-28]

In this work, we performed amplitude-distance spectroscopy and MD simulations of AM-AFM of two different self-assembled monolayers (SAMs) in water, where the hydrophilicity or hydrophobicity of the SAMs was determined by the terminal group of the alkanethiols. The hydration structures near both surfaces were analyzed using the simulations. Then, the amplitude of tip oscillation as a function of distance from the SAMs was obtained from both simulations and experiments. The two SAMs had similar molecular lengths as well as surface packing, so differences in the force spectroscopy data could be attributed to interactions between the tip and the terminal groups. Based on the atomic-scale information from the simulations, the relationship between the amplitude and distance was analyzed in terms of the interaction force between the tip and the water, as well as between the tip and the SAMs, and trends were associated with the hydration structure near the SAM-water interface. The results may enable better understanding of AM-AFM measurements of interfacial phenomena on various surfaces in water.

METHODS

Monolayer Self Assembly. Unless otherwise stated, all materials were purchased from Fisher Scientific Co. (Pittsburg, PA, USA). Water was supplied from a NANOpure Diamond (Barnstead, Lake Balboa, CA, USA) with a resistivity of 18.2 MΩ • cm. All glassware was cleaned with piranha acid (3:1 H_2SO_4:H_2O_2) rinsed with water and dried with compressed air filtered with Vacu-Guard L#S975 (GE Whatman, Pittsburgh, PA, USA). Au (111) bead substrates were prepared

using a standard protocol.[29] The substrates were cleaned with hot nitric acid (CAUTION: hot nitric acid is highly corrosive and reacts violently with organics), rinsed with water, and flame annealed in a H_2 flame before they were immersed in the corresponding ethanolic solutions (4 mM 11-mercapto-1-undecanol or 1-dodecanethiol, Sigma-Aldrich Co., St. Louis, MO, USA) in the dark and under nitrogen (Praxair Inc., Danbury, CT, USA) for 24 h. Prior to imaging, the surfaces were rinsed with ethanol, then water, and dried with compressed air. The samples were secured to a custom-made AFM Teflon liquid cell that was cleaned with piranha (3:1 sulfuric acid: 30% hydrogen peroxide. CAUTION— piranha is highly corrosive and reacts violently with organics), rinsed with water, and dried with compressed air.

Force Spectroscopy and Imaging. Amplitude spectra and imaging was performed with the sample under 1-2 mL pH 7 4-(2-hydroxyethyl)-1-piperazineethanesulfonic acid (HEPES) buffer solution (170 mM KCl, 10 mM HEPES). The HEPES buffer solution was used to stabilize the pH and screen long range electrostatic forces that would mask the van der Waals attractive forces and observable hydration structures.[30] All force spectroscopy and imaging data were obtained with an Agilent/Keysight 5500 AFM (Keysight Technologies, Santa Rosa, CA, USA) modified for non-contact AM-AFM[31] equipped with PPP-NCSTAuD (spring constants 7.4 N/m listed, 3-4 N/m measured, Nanosensors, Neuchâtel, Switzerland) cantilevers that were cleaned with SC-1 (5:1:1 water:NH_4OH:H_2O_2) for 1 minute then rinsed with water then placed to dry in a covered glass container and rinsed with previously mentioned buffer solution prior to use. Cantilevers were acoustically driven at their resonance frequencies of approximately 45-55 kHz. The approach was set for 1 μm/s to a setpoint of 80% of the free amplitude, once the surface was reached the tip was withdrawn 1 μm, amplitude lowered, then re-approached to a setpoint of 92% of free amplitude.[32] Amplitude-distance curves were collected with PicoView 2.0 (Keysight Technologies, Santa Rosa,

CA, USA). The amplitude-distance curves were measured with distance limits relative to z-piezo position at setpoint amplitude (upper limits 1 to 2 nm, lower limits -1 to -2 nm). Images were processed with WSxM.[33]

Molecular Dynamics Simulation. The MD model consisted of a truncated hemispheric diamond AFM tip apex and a SAM surface immersed in water, as shown in Figure 1(a). The radius of the tip was 1.5 nm and the height of spherical cap was 1.5 nm. The alkanethiol (-$S(CH_2)_{11}X$, X) SAMs were terminated with either -CH_3, for a hydrophobic surface, or –OH, for a hydrophilic surface. Both types of SAMs were placed on an atomically flat Au (111) surface with dimensions 5.0 nm × 5.2 nm in the x and y directions. The sulfur head groups of the SAM molecules formed a $\left(\sqrt{3} \times \sqrt{3}\right)R30^{\circ}$ two-dimensional triangular lattice on the gold surface with a surface density of 0.216 nm^2 per chain, consistent with previous experiments and simulations.[34-36] The distance in the z direction between the gold surface and the sulfur head group of each alkanethiol was held constant at 0.238 nm.[34, 37]

We used the united atom model for the CH_2 and CH_3 groups in the 1-dodecanethiol (C12) and 11-mercapto-1-undecanol (C11OH) SAMs, so the hydrogen atoms were treated implicitly with their masses lumped into the corresponding carbon atoms. This method is computationally efficient and provides enough accuracy for quantitative analysis based on previous results for the Au-SAM system.[34, 36, 38-39] In the united atom model, the intramolecular interactions within the molecule were described with parameters from [39]. To model the hydroxyl terminated C11OH SAMs, partial charges and potential parameters for the O and H atoms were taken from [40]. The interactions within the tip and the gold substrate were described by the adaptive intermolecular reactive empirical bond order (AIREBO) potential[41] and the embedded atom method (EAM),[42] respectively.

The water model used in this study was the extended Simple Point Charge potential SPC/E,[43] which is known to reproduce the structure and dynamics of bulk water.[44] The Morse potential was used to describe the interactions between the S and Au atoms.[45-46] All other long-range interactions were modeled using the Lennard-Jones potential with parameters from [39] and the Lorentz–Berthelot mixing rules.[47] All simulations were run using large-scale atomic/molecular massively parallel simulator (LAMMPS)[48] software with a time step of 0.25 fs.

To validate the model and interaction potentials, we first simulated just the SAMs on a flat Au (111) surface and calculated the tilt angle of the molecules. The system was relaxed at 300 K for 10 ns in the NVT ensemble (constant number, volume and temperature). An average tilt angle of $(27.1 \pm 2.5)°$ and $(27.0 \pm 4.1)°$ was observed for C12 and C11OH SAMs, respectively. This agrees with the tilt angle of $(30 \pm 10)°$ measured from pervious experiments and simulations.[34, 49-51]

We used an MD approach developed previously to simulate AM-AFM.[52-53] The tip was connected to a virtual atom through a harmonic spring with stiffness 40 N/m in the z direction. The top 0.4 nm of the tip was treated as rigid body and the bottom 0.1 nm of the Au substrate was fixed. Periodic boundary conditions were applied in the x and y directions. The system was first relaxed at 300 K in the NVT ensemble for 50 ps. The temperature was controlled by applying a Nosé-Hoover thermostat to all non-constrained atoms. Then equilibration was performed at 300 K and 100 kPa in the NPT (constant number, pressure and temperature) ensemble for 50 ps. Finally, a 50-ps NVT simulation at 300 K was performed. During this last stage of equilibration, the number densities of oxygen atoms in the water and the carbon or oxygen atoms in the SAMs in bins perpendicular to the surface were averaged. Then the virtual atom was oscillated with an amplitude of 0.1 nm and a frequency of 91 GHz. Previous research has shown that the amplitude of tip

oscillation varies with frequency, first increasing, reaching a maximum value and then decreasing with increasing frequency.[5] This trend was observed in the simulations here and used to select a frequency of 91 GHz to maximize the amplitude. The large frequency of the excitation signal was necessitated by the timescale limitations of MD simulations.[53] The quality factor Q, which is the ratio of the free amplitude of tip oscillation to the driving amplitude of virtual atom, was estimated to be 1.3. This low quality factor can be attributed to the contribution of the surrounding fluid to the overall damping[54] and is on the same order of magnitude of previous AM-AFM experiments in aqueous solution.[55] The ensemble of tip and virtual atom was placed above the SAM surface at different vertical positions to obtain the relationship between the oscillation amplitude of the tip and its vertical position.

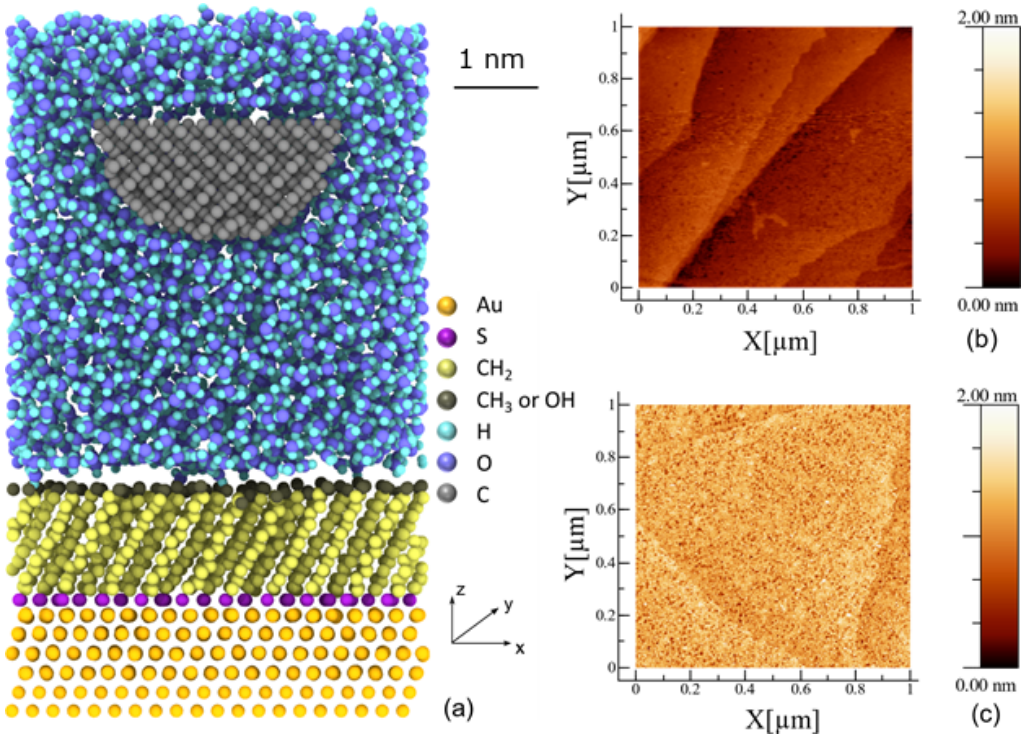

Figure 1: (a) Cross sectional view of the model showing the tip apex in water and SAMs on a gold surface. Topography measured experimentally with AM-AFM of (b) the C12 SAM surface and (c)

the C11OH SAM surface. The phase images (Figure S6) show uniform surface chemistry for each surface.

RESULTS AND DISCUSSION

To investigate the interactions between the SAM surface and water, we calculated the number density profiles of the water and SAMs, as shown in Figures 2(a) and (b), for the hydrophobic C12 SAM and hydrophilic C11OH SAM surfaces, respectively. The vertical position z is defined as the center of mass of the volume of atoms used for calculating number density, where z=0 is the top of the SAMs. The density was normalized by the maximum value for the water and the SAMs separately. It can be seen that, near the SAM surface, the water density oscillates along the vertical direction, which indicates layering of the water near the surface for both C12 and C11OH SAMs. The distance between the peaks of the water density profile, identified by arrows in Figures 2(a) and (b), is ~0.3 nm for both surfaces, which corresponds to approximately the diameter of one water molecule. The formation of this hydration structure and the distance between hydration layers are consistent with the water structure at other interfaces studied using experiments and simulations.[27, 56] In addition, as shown in the dashed boxes in Figures 2(a) and (b), there is a larger overlap between the density profile of water and the C11OH surface than the density profile of water and the C12 surface. This is consistent with the snapshots from simulations shown as insets in Figures 2(a) and (b) where the water is closer to the C11OH surface than to the C12 surface. This observation is in agreement with previous experimental and simulation studies,[27, 57] and can be attributed to attractive electrostatic interactions between the hydroxyl groups and water.

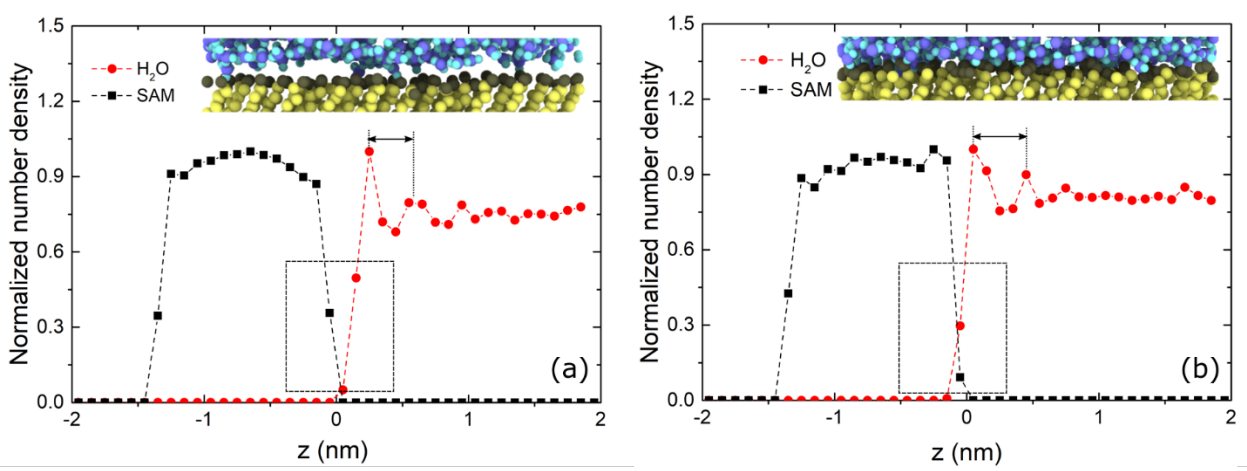

Figure 2: Normalized number density profiles of water and SAMs for (a) C12 SAM and (b) C11OH SAM. The insets show snapshots of the water-SAM interface after equilibration.

Understanding how the hydration structures resulting from different surface chemistries impact oscillation amplitude is important since amplitude, the feedback signal for AM-AFM, is one of key factors that determine atomic scale contrast. We characterized the amplitude as a function of distance from the SAM surfaces in both experiments and simulations. Figure 3 shows the amplitude as a function of the vertical position of the cantilever in experiments and the virtual atom in simulations. It can be seen that, in both experiments and simulation, when the tip was far away from the SAM surface ($z > 2$ nm), the amplitude plateaued to a value corresponding to the free oscillation amplitude, where the tip dynamic response was only determined by the excitation signal. The free amplitude was $A_0 \approx 1$ nm in experiments and $A_0 = 0.13$ nm in simulations. As the tip approached the SAM surface, the amplitude of oscillation decreased due to the interactions between the tip and SAM surface. Eventually, the tip was in contact with the SAM surface and the amplitude decreased to zero. This trend of amplitude as a function of cantilever vertical position is consistent with previous studies of AM-AFM in air.[58]

A peak in the amplitude-distance curve is observed between the free oscillation regime and the hard contact regime for C12 in both experimental and simulated amplitude profiles (Figures 3(a) and 3(c)). However, C11OH does not exhibit such features (Figures 3(b) and (d)). Comparing the results from experiments and simulations in Figure 3, differences in magnitude can be observed and are likely attributable to discrepancies in oscillation frequency, amplitude, spring stiffness, and tip material. Another complication is that the force spectra may be also influenced by the nanoscale structure of the tip apex in the experiment, which is largely unknown. Therefore, in each of the force spectroscopy experiments, we performed measurements of the two surfaces in various sequences, with the same tip used for measurements within each sequence: C12 - C11OH, C11OH - C12, C12 - C11OH - C12, and C11OH - C12 - C11OH (Supporting Information). Comparing the results from different sequences (different tips), variability in the magnitude as well as the position of the peak was observed. However, regardless of the sequence of the measurements or the tip used, the experimental force spectra of C12 SAM consistently exhibited a peak between the free oscillation regime and hard contact regime, while C11OH did not.

It should be noted that nanobubbles may form on hydrophobic SAMs like C12, complicating the interpretation of the amplitude vs distance curves.[59-60] Nanobubbles were not observed under the imaging and force spectroscopy conditions used in this study. However, a small number of nanobubbles were observed in measurements taken with a softer cantilever (0.35 N/m) as shown in Figure S7. Consistent with previous studies, the heights of these bubbles ranged from a few to ten nanometers. However, the presence of nanobubbles cannot explain the major features observed here. In particular, the long-range attractive interactions caused by the presence of a nanobubble should lead to peaks even when the tip is a few to tens of nanometers away from the surface. Such features were not observed in most amplitude *vs*. distance curves. Moreover, nanobubbles are

known to occupy only a fraction of the surface[59-60] and hence cannot account for the consistent appearance of peaks in the amplitude-distance curves on the C12 SAM. Therefore, the spectra reflect the short-range interaction between the SAMs and the tip apex in water and we conclude that the different surface functional groups (methyl vs. hydroxyl) are responsible for the difference in the amplitude *vs* distance curves.

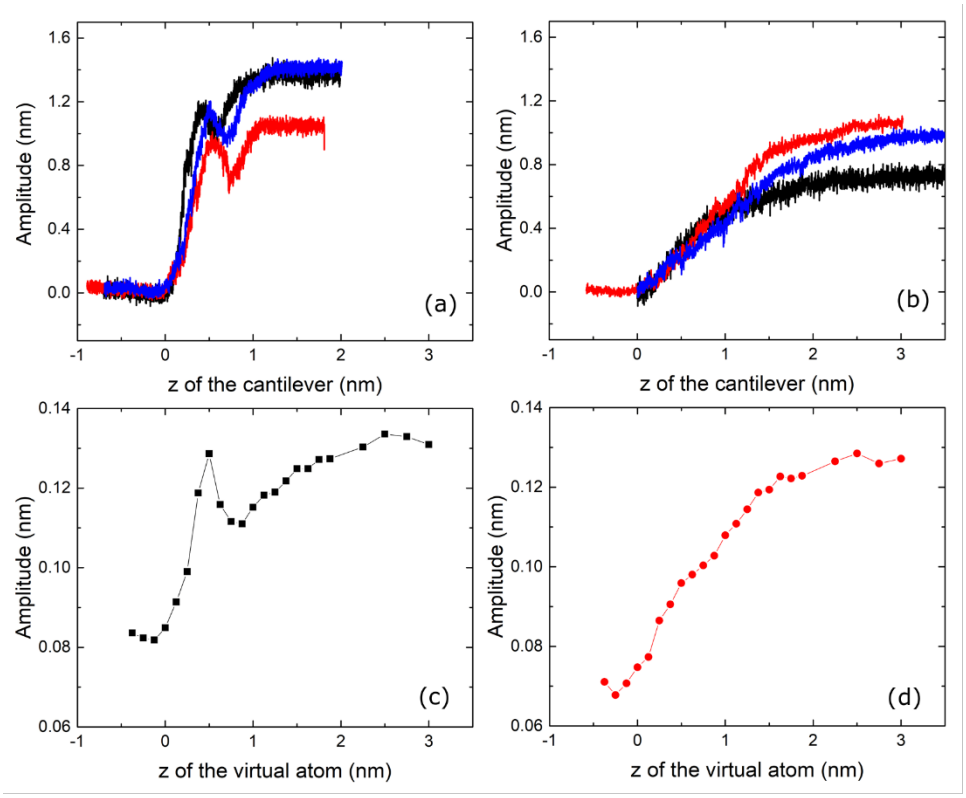

Figure 3: Amplitude as a function of cantilever/virtual atom position for: (a) C12 surface in experiments, (b) C11OH surface in experiments, (c) C12 surface in simulations, and (d) C11OH surface in simulations. The three data sets in the results from experiments represent three repeated tests performed on the same surface with the same tip.

To understand the differences between the force spectra of the two surfaces, we isolated the contributions to the force that the tip experienced. The model tip was placed at different vertical positions and the system was relaxed for 250 ps to calculate the z-component of the forces acting on the tip. The average values of the total force, force due only to interactions with water and force due only to interactions with the tip were calculated.

As shown in Figure 4(a), the total force that the tip experienced differed for the two SAM surfaces. Specifically, the tip experienced a large net attractive (negative) force close to the C12 SAMs, which was not observed for the C11OH SAMs. This difference can be understood by analyzing the individual contributions of the water and the SAMs. As shown in Figure 4(b), on both surfaces, the SAMs did not contribute to the total force when the bottom of the tip was at least 0.6 nm away from the SAM surface. As the tip approached the SAM surface, the tip started to experience an attractive force from the SAM, followed by a repulsive force when the tip continued to move downwards. The maximum adhesive force (largest negative force) appeared when the tip was closer to the C11OH surface than the C12 surface. This can be attributed to the fact that the first hydration layer was closer to the C11OH surface than the C12 surface (Figure 2). In addition, from Figure 4(c), it can be seen that, as the tip approached the C11OH surface, the tip experienced a large repulsive force from the water molecules, which is consistent with previous studies on hydrophilic surfaces.[22-23] However, this repulsion was small when the tip approached the C12 surface. Thus, there was an attractive force from the SAMs on both surfaces, but this was counter-balanced by a repulsive force from the water on the hydrophilic SAMs such that there was no net attractive force on the tip in this case.

The force results may explain the differences in tip amplitude for the two surfaces shown in Figure 3. A discontinuity in the amplitude curve has been attributed to a transition between attractive and

repulsive force regimes.[61] It has been suggested that this discontinuity is more likely to happen for stiff materials and small free-oscillation amplitudes.[61] From Figures 3(c) and 4(a), it can be seen that the amplitude spike for the C12 surface occurred when the tip started to experience an attractive force. Thus, the attractive force the tip experienced near the C12 surface resulted in a distinct feature in the amplitude curve. This feature did not appear on the C11OH surface because the tip did not experience a net attractive force, so there was no transition from the attractive to the repulsive regime.

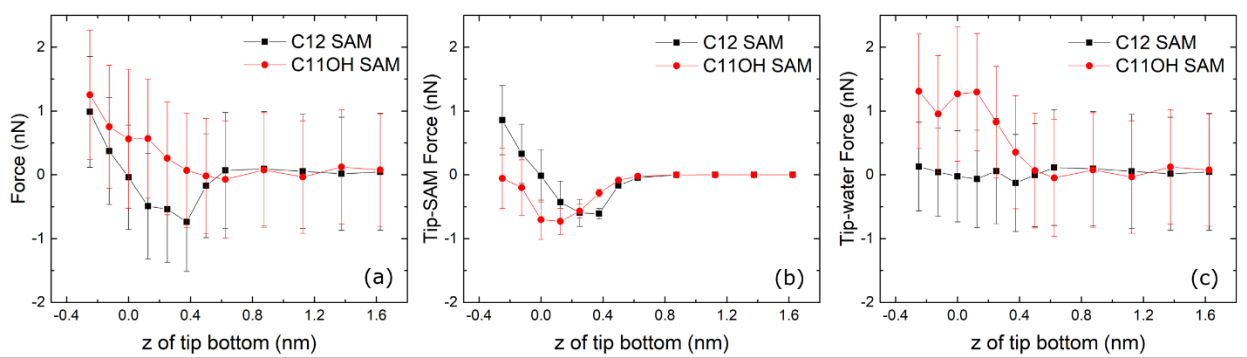

Figure 4: The force that the model tip experienced at different vertical positions, where z is the position of the bottom of the tip: (a) total force on the tip, (b) interaction force between the tip and SAM surface, and (c) interaction force between the tip and water.

CONCLUSIONS

In summary, we have presented results from MD simulations to complement AM-AFM measurements of SAMs to investigate the relationship between the amplitude of tip oscillation and tip-sample distance. The terminal group of the SAMs was varied and both experimental and simulated results exhibited similar trends in the amplitude-distance curve. By combining experimental AM-AFM measurements and MD simulations, this study provides atomic-scale

information about the water-SAM interface system to interpret the relationship between the structure of the hydration layer, the force that the tip experiences during a measurement, and amplitude of tip oscillation. Different surface chemistries were observed to produce substantially different short-range tip-surface interactions and amplitude distance curves. These results raise intriguing questions regarding the impact of such subnanometer scale tip-surface interactions on the subnanometer scale imaging contrast of surfaces in aqueous environments.[62-63] Future studies that systematically explore the relationship between amplitude, phase, and surface functionality on nanopatterned surfaces may lead to a more comprehensive understanding of how surface chemistry changes the water structure and tip-sample interaction forces, and set the stage for in situ subnanometer resolution imaging of a variety of functionalized surfaces. [62, 64-66]

ASSOCIATED CONTENT

Supporting Information.

Experimental amplitude-distance curves from other measurements

AUTHOR INFORMATION

Corresponding Author

*Email: tye2@ucmerced.edu (T.Y.).
*Email: amartini@ucmerced.edu (A.M.).

Notes

The authors declare no competing financial interest.

ACKNOWLEDGMENT

This research was supported by the NASA Merced nanomaterials Center for Energy and Sensing (MACES) through the support of the National Aeronautics and Space Administration (NASA) grant no. NNX15AQ01.

REFERENCES

1. Magonovº, S.; Elings, V.; Whangbo, M., Phase imaging and stiffness in tapping-mode atomic force microscopy. *Surf. Sci.* **1997,** *375*, L385-L391.
2. Giessibl, F. J., Atomic resolution of the silicon (111)-(7x7) surface by atomic force microscopy. *Science* **1995,** *267* (5194), 68-71.
3. Rief, M.; Oesterhelt, F.; Heymann, B.; Gaub, H. E., Single molecule force spectroscopy on polysaccharides by atomic force microscopy. *Science* **1997,** *275* (5304), 1295-1297.
4. Giessibl, F. J., Advances in atomic force microscopy. *Rev. Mod. Phys.* **2003,** *75* (3), 949.
5. Garcıa, R.; Perez, R., Dynamic atomic force microscopy methods. *Surf. Sci. Rep.* **2002,** *47* (6-8), 197-301.
6. Weisenhorn, A.; Hansma, P.; Albrecht, T.; Quate, C., Forces in atomic force microscopy in air and water. *Appl. Phys. Lett.* **1989,** *54* (26), 2651-2653.
7. Voïtchovsky, K.; Kuna, J. J.; Contera, S. A.; Tosatti, E.; Stellacci, F., Direct mapping of the solid–liquid adhesion energy with subnanometre resolution. *Nat. Nanotechnol.* **2010,** *5* (6), 401.
8. Umeda, K.; Zivanovic, L.; Kobayashi, K.; Ritala, J.; Kominami, H.; Spijker, P.; Foster, A. S.; Yamada, H., Atomic-resolution three-dimensional hydration structures on a heterogeneously charged surface. *Nat. Commun.* **2017,** *8* (1), 2111.
9. Kuna, J. J.; Voïtchovsky, K.; Singh, C.; Jiang, H.; Mwenifumbo, S.; Ghorai, P. K.; Stevens, M. M.; Glotzer, S. C.; Stellacci, F., The effect of nanometre-scale structure on interfacial energy. *Nat. Mater.* **2009,** *8* (10), 837.
10. Sugimoto, Y.; Pou, P.; Abe, M.; Jelinek, P.; Pérez, R.; Morita, S.; Custance, O., Chemical identification of individual surface atoms by atomic force microscopy. *Nature* **2007,** *446* (7131), 64.
11. Cleveland, J.; Schäffer, T.; Hansma, P., Probing oscillatory hydration potentials using thermal-mechanical noise in an atomic-force microscope. *Phys. Rev. B* **1995,** *52* (12), R8692.
12. Carrasco, J.; Hodgson, A.; Michaelides, A., A molecular perspective of water at metal interfaces. *Nat. Mater.* **2012,** *11* (8), 667.
13. Ebeling, D.; Solares, S. D., Amplitude modulation dynamic force microscopy imaging in liquids with atomic resolution: comparison of phase contrasts in single and dual mode operation. *Nanotechnology* **2013,** *24* (13), 135702.
14. Martin-Jimenez, D.; Garcia, R., Identification of Single Adsorbed Cations on Mica–Liquid Interfaces by 3D Force Microscopy. *J. Phys. Chem. Lett.* **2017,** *8* (23), 5707-5711.

15. Martin-Jimenez, D.; Chacon, E.; Tarazona, P.; Garcia, R., Atomically resolved three-dimensional structures of electrolyte aqueous solutions near a solid surface. *Nat. Commun.* **2016,** *7*, 12164.
16. Herruzo, E. T.; Asakawa, H.; Fukuma, T.; Garcia, R., Three-dimensional quantitative force maps in liquid with 10 piconewton, angstrom and sub-minute resolutions. *Nanoscale* **2013,** *5* (7), 2678-2685.
17. Ishida, N.; Inoue, T.; Miyahara, M.; Higashitani, K., Nano bubbles on a hydrophobic surface in water observed by tapping-mode atomic force microscopy. *Langmuir* **2000,** *16* (16), 6377-6380.
18. Walczyk, W.; Hain, N.; Schönherr, H., Hydrodynamic effects of the tip movement on surface nanobubbles: a combined tapping mode, lift mode and force volume mode AFM study. *Soft Matter* **2014,** *10* (32), 5945-5954.
19. **!!! INVALID CITATION !!!** {}.
20. Fukuma, T.; Reischl, B.; Kobayashi, N.; Spijker, P.; Canova, F. F.; Miyazawa, K.; Foster, A. S., Mechanism of atomic force microscopy imaging of three-dimensional hydration structures at a solid-liquid interface. *Phys. Rev. B* **2015,** *92* (15), 155412.
21. Reischl, B.; Watkins, M.; Foster, A. S., Free energy approaches for modeling atomic force microscopy in liquids. *J. Chem. Theory Comput.* **2012,** *9* (1), 600-608.
22. Kobayashi, K.; Liang, Y.; Amano, K.-i.; Murata, S.; Matsuoka, T.; Takahashi, S.; Nishi, N.; Sakka, T., Molecular dynamics simulation of atomic force microscopy at the water–muscovite interface: hydration layer structure and force analysis. *Langmuir* **2016,** *32* (15), 3608-3616.
23. Argyris, D.; Ashby, P. D.; Striolo, A., Structure and orientation of interfacial water determine atomic force microscopy results: Insights from molecular dynamics simulations. *ACS Nano* **2011,** *5* (3), 2215-2223.
24. Argyris, D.; Phan, A.; Striolo, A.; Ashby, P. D., Hydration structure at the α-Al2O3 (0001) surface: Insights from experimental atomic force spectroscopic data and atomistic molecular dynamics simulations. *J. Phys. Chem. C* **2013,** *117* (20), 10433-10444.
25. Miyazawa, K.; Kobayashi, N.; Watkins, M.; Shluger, A. L.; Amano, K.-i.; Fukuma, T., A relationship between three-dimensional surface hydration structures and force distribution measured by atomic force microscopy. *Nanoscale* **2016,** *8* (13), 7334-7342.
26. Fukuma, T.; Higgins, M. J.; Jarvis, S. P., Direct imaging of lipid-ion network formation under physiological conditions by frequency modulation atomic force microscopy. *Phys. Rev. Lett.* **2007,** *98* (10).
27. Jensen, M. Ø.; Mouritsen, O. G.; Peters, G. H., The hydrophobic effect: Molecular dynamics simulations of water confined between extended hydrophobic and hydrophilic surfaces. *J. Chem. Phys.* **2004,** *120* (20), 9729-9744.
28. Lee, S. H.; Rossky, P. J., A comparison of the structure and dynamics of liquid water at hydrophobic and hydrophilic surfaces—a molecular dynamics simulation study. *J. Chem. Phys.* **1994,** *100* (4), 3334-3345.
29. Clavilier, J.; Faure, R.; Guinet, G.; R, D., Preparation of monocrystalline Pt microelectrodes and electrochemical study of the plane surfaces cut in the direction of the {111} and {110} planes. *Journal of Electroanalytical Chemistry and Interfacial Electrochemistry* **1980,** *107*, 205-209.
30. Butt, H. J., Measuring electrostatic, van der Waals, and hydration forces in electrolyte solutions with an atomic force microscope. *Biophys J* **1991,** *60* (6), 1438-44.

31. Fukuma, T.; Kimura, M.; Kobayashi, K.; Matsushige, K.; Yamada, H., Development of low noise cantilever deflection sensor for multienvironment frequency-modulation atomic force microscopy. *Rev Sci Instrum* **2005,** *76*.
32. Miller, E. J.; Trewby, W.; Farokh Payam, A.; Piantanida, L.; Cafolla, C.; Voïtchovsky, K., Sub-nanometer Resolution Imaging with Amplitude-modulation Atomic Force Microscopy in Liquid. *J Vis Exp* **2016,** (118).
33. Horcas, I.; Fernández, R.; Gómez-Rodríguez, J. M.; Colchero, J.; Gómez-Herrero, J.; Baro, A. M., WSXM: a software for scanning probe microscopy and a tool for nanotechnology. *Rev Sci Instrum* **2007,** *78* (1), 013705.
34. Ghorai, P. K.; Glotzer, S. C., Molecular dynamics simulation study of self-assembled monolayers of alkanethiol surfactants on spherical gold nanoparticles. *J. Phys. Chem. C* **2007,** *111* (43), 15857-15862.
35. Hinterwirth, H.; Kappel, S.; Waitz, T.; Prohaska, T.; Lindner, W.; Lämmerhofer, M., Quantifying thiol ligand density of self-assembled monolayers on gold nanoparticles by inductively coupled plasma–mass spectrometry. *ACS Nano* **2013,** *7* (2), 1129-1136.
36. Majumdar, S.; Sierra-Suarez, J. A.; Schiffres, S. N.; Ong, W.-L.; Higgs III, C. F.; McGaughey, A. J.; Malen, J. A., Vibrational mismatch of metal leads controls thermal conductance of self-assembled monolayer junctions. *Nano Lett.* **2015,** *15* (5), 2985-2991.
37. Majumder, C.; Briere, T. M.; Mizuseki, H.; Kawazoe, Y., Structural investigation of thiophene thiol adsorption on Au nanoclusters: Influence of back bonds. *J. Chem. Phys.* **2002,** *117* (6), 2819-2822.
38. Henz, B. J.; Fischer, J. W.; Zachariah, M. R. *Molecular Simulations of Gold Nanoparticles Coated With Self-Assembled Alkanethiolate Monolayers*; ARMY RESEARCH LAB ABERDEEN PROVING GROUND MD: 2006.
39. Ong, W.-L.; Majumdar, S.; Malen, J. A.; McGaughey, A. J., Coupling of organic and inorganic vibrational states and their thermal transport in nanocrystal arrays. *J. Phys. Chem. C* **2014,** *118* (14), 7288-7295.
40. Hautman, J.; Bareman, J. P.; Mar, W.; Klein, M. L., Molecular dynamics investigations of self-assembled monolayers. *J. Chem. Soc. Faraday Trans.* **1991,** *87* (13), 2031-2037.
41. Stuart, S. J.; Tutein, A. B.; Harrison, J. A., A reactive potential for hydrocarbons with intermolecular interactions. *J. Chem. Phys.* **2000,** *112* (14), 6472-6486.
42. Grochola, G.; Russo, S. P.; Snook, I. K., On fitting a gold embedded atom method potential using the force matching method. *J. Chem. Phys.* **2005,** *123* (20), 204719.
43. Berendsen, H.; Grigera, J.; Straatsma, T., The missing term in effective pair potentials. *J. Phys. Chem.* **1987,** *91* (24), 6269-6271.
44. Vega, C.; Abascal, J. L., Simulating water with rigid non-polarizable models: a general perspective. *Phys. Chem. Chem. Phys.* **2011,** *13* (44), 19663-19688.
45. Mahaffy, R.; Bhatia, R.; Garrison, B. J., Diffusion of a butanethiolate molecule on a Au {111} surface. *J. Phys. Chem. B* **1997,** *101* (5), 771-773.
46. Sung, I.-H.; Kim, D.-E., Molecular dynamics simulation study of the nano-wear characteristics of alkanethiol self-assembled monolayers. *Appl. Phys. A* **2005,** *81* (1), 109-114.
47. Allen, M. P.; Tildesley, D. J., *Computer Simulation of Liquids*. Oxford university press: 2017.
48. Plimpton, S., Fast parallel algorithms for short-range molecular dynamics. *J. Comput. Phys.* **1995,** *117* (1), 1-19.

49. Porter, M. D.; Bright, T. B.; Allara, D. L.; Chidsey, C. E., Spontaneously organized molecular assemblies. 4. Structural characterization of n-alkyl thiol monolayers on gold by optical ellipsometry, infrared spectroscopy, and electrochemistry. *J. Am. Chem. Soc.* **1987,** *109* (12), 3559-3568.
50. Nuzzo, R. G.; Dubois, L. H.; Allara, D. L., Fundamental studies of microscopic wetting on organic surfaces. 1. Formation and structural characterization of a self-consistent series of polyfunctional organic monolayers. *J. Am. Chem. Soc.* **1990,** *112* (2), 558-569.
51. Vemparala, S.; Karki, B. B.; Kalia, R. K.; Nakano, A.; Vashishta, P., Large-scale molecular dynamics simulations of alkanethiol self-assembled monolayers. *J. Chem. Phys.* **2004,** *121* (9), 4323-4330.
52. Hu, X.; Chan, N.; Martini, A.; Egberts, P., Tip convolution on HOPG surfaces measured in AM-AFM and interpreted using a combined experimental and simulation approach. *Nanotechnology* **2016,** *28* (2), 025702.
53. Hu, X.; Egberts, P.; Dong, Y.; Martini, A., Molecular dynamics simulation of amplitude modulation atomic force microscopy. *Nanotechnology* **2015,** *26* (23), 235705.
54. Xu, R.-G.; Leng, Y., Contact stiffness and damping of liquid films in dynamic atomic force microscope. *J. Chem. Phys.* **2016,** *144* (15), 154702.
55. Marutschke, C.; Walters, D.; Cleveland, J.; Hermes, I.; Bechstein, R.; Kühnle, A., Three-dimensional hydration layer mapping on the (10.4) surface of calcite using amplitude modulation atomic force microscopy. *Nanotechnology* **2014,** *25* (33), 335703.
56. Zhou, H.; Ganesh, P.; Presser, V.; Wander, M. C.; Fenter, P.; Kent, P. R.; Jiang, D.-e.; Chialvo, A. A.; McDonough, J.; Shuford, K. L., Understanding controls on interfacial wetting at epitaxial graphene: Experiment and theory. *Phys. Rev. B* **2012,** *85* (3), 035406.
57. Shenogina, N.; Godawat, R.; Keblinski, P.; Garde, S., How wetting and adhesion affect thermal conductance of a range of hydrophobic to hydrophilic aqueous interfaces. *Phys. Rev. Lett.* **2009,** *102* (15), 156101.
58. Strus, M. C.; Raman, A.; Han, C.; Nguyen, C., Imaging artefacts in atomic force microscopy with carbon nanotube tips. *Nanotechnology* **2005,** *16* (11), 2482.
59. Walczyk, W.; Schon, P. M.; Schonherr, H., The effect of PeakForce tapping mode AFM imaging on the apparent shape of surface nanobubbles. *J Phys-Condens Mat* **2013,** *25* (18).
60. Song, B.; Walczyk, W.; Schonherr, H., Contact Angles of Surface Nanobubbles on Mixed Self-Assembled Monolayers with Systematically Varied Macroscopic Wettability by Atomic Force Microscopy. *Langmuir* **2011,** *27* (13), 8223-8232.
61. Garcia, R.; San Paulo, A., Attractive and repulsive tip-sample interaction regimes in tapping-mode atomic force microscopy. *Phys. Rev. B* **1999,** *60* (7), 4961.
62. Inada, N.; Asakawa, H.; Matsumoto, Y.; Fukuma, T., Molecular-scale surface structures of oligo (ethylene glycol)-terminated self-assembled monolayers investigated by frequency modulation atomic force microscopy in aqueous solution. *Nanotechnology* **2014,** *25* (30).
63. Fukuma, T., Water distribution at solid/liquid interfaces visualized by frequency modulation atomic force microscopy. *Science and Technology of Advanced Materials* **2010,** *11* (3), 033003.
64. Hao, X.; Josephs, E. A.; Gu, Q.; Ye, T., Molecular conformations of DNA targets captured by model nanoarrays. *Nanoscale* **2017,** *9* (36), 13419-13424.
65. Abel, G. R., Jr.; Josephs, E. A.; Luong, N.; Ye, T., A switchable surface enables visualization of single DNA hybridization events with atomic force microscopy. *J. Am. Chem. Soc.* **2013,** *135* (17), 6399-6402.

66. Josephs, E. A.; Ye, T., A single-molecule view of conformational switching of DNA tethered to a gold electrode. *J. Am. Chem. Soc.* **2012,** *134* (24), 10021-10030.

For Table of Contents Only